Comparing brine-seawater mixing between two-port and four-port rotary energy recovery device

Enle Xu[a,b], Xiaofeng Jiang[a], Zhenyong Miao[a,*], Fenglei Wang[c]

[a]*School of Chemical Engineering and Technology, China University of Mining and Technology, Xuzhou, Jiangsu, 221116, P.R. China, emails: zymiao@cumt.edu.cn (Z. Miao), xel360@126.com (E. Xu), jiangxf8822@163.com (X. Jiang)*
[b]*College of Electromechanical Engineering, Qingdao University of Science and Technology, Qingdao 266061, P.R. China*
[c]*Qingdao Changlong Power Equipment Co., Ltd., Qingdao 266700, China, email: wangfenglei0730@163.com*

ABSTRACT

In order to compare the mixing behavior between two-port and four-port rotary energy recovery device (RERD), the effect of operational conditions on mixing of two-port RERD was investigated by CFD simulation. The sliding mesh technique and species transport equations which had been verified by our previous research were used in the simulation process, indicates that the simulation result is reasonable. New method was proposed to calculate the inflow length based on NaCl mass fractions of two rotor ducts in sealed zone. Inflow length of two-port RERD is about twice as long as that of four-port RERD under the same rotor speed and flow rate. Simulation results revealed that two-port RERD exhibits polynomial relation between mixing and dimensionless inflow length, the same trend with four-port RERD. When mixing of two-port or four-port RERD is controlled in level of 6%, dimensionless inflow length must be less than 0.76. Four-port RERD facilitates to keep the mixing in a less level compared with two-port RERD, which is the developing trend for the RERD. The work can give some insights into the mixing difference between two-port RERD and four-port RERD, and guide the design of RERD in a low level mixing.

Keywords: Rotary energy recovery device; CFD; Mixing; Inflow length

1. Introduction

In order to remit the global problem of water shortage, seawater reverse osmosis desalination (SWRO) is an important water desalination technology [1–4]. Rotary energy recovery device (RERD) is one of the indispensable devices to reduce the operating cost about 50% or higher when the water productivity of SWRO is about 40%–45% [5–7]. RERD is a typical example of the positive displacement energy recovery device [8–10]. RERD transfer pressure energy directly from high pressure (HP) brine to low pressure (LP) seawater with the efficiency of above 90%. The brine contact directly with seawater in rotor ducts, so it is inevitable for brine-seawater mixing in RERD [11]. Therefore, it is of great significance to investigate how to keep the mixing in a less level.

Stover et al. [12,13] proposed that the interface between brine and seawater never reaches the rotor duct end before the duct are sealed. Zhou et al. [14] showed that mixing zone moves reciprocally in the duct whose moving distance is almost unchanged. Liu et al. [15] presented that the liquid piston divides water and brine to hold back over-mixing. The mixing rises with the increase of flow rate and decrease of rotation speed. Stover [16] and Mambretti et al. [17] showed that the mixing has relation with rotation speed, which is in its turn a function of the streams velocity.

* Corresponding author.

Cao et al. [18] implemented the CFD method coupling with residence time distribution analysis to study the mixing performance and flow filled of RERD in different operational conditions. The mixing was minimized at an oscillatory Reynolds number of 178. Wang et al. [19] analyzed the concentration distribution of five kinds of rotary pressure exchangers which have different sizes and structures utilized the Fluent software. Simulation results revealed that the model size, rotor duct number, and endcover structure have influence on the volumetric mixing.

Though some researchers pointed out the operational conditions and the structures of the RERD are the major parameters affected the mixing, few researchers pay attention to the specific function between the mixing and operational conditions. In addition, RERD can divide into two-port and four-port RERD according to the port number in the end plate. For the two/four-port RERD, the seawater or brine end plate embodies two/four ports, one/two ports for HP fluid and the other for LP fluid. Furthermore, the mixing difference between two-port and four-port RERD is still scarce.

Our previous study [20] focused on the relation between operational conditions and mixing behavior of the four-port RERD and built the function between mixing and dimensionless flow length. The paper seeks to investigate the rotor speed and the stream velocity on mixing for two-port RERD according to four-port RERD simulation method, and compare the mixing difference between two-port and four-port RERD.

2. Operational principle of the RERD

Fig. 1 provides the operational principle of the SWRO with RERD. The LP seawater was taken out from the sea by the seawater water pump. A part of seawater was pressurized by high pressure pump. The other part obtained the pressure energy from the HP brine thought RERD, and then re-pressurized by the booster pump. The HP seawater which flowed out from high pressure pump and booster pump fed into membrane modules, and divided into fresh water and HP brine.

The key units of RERD are seawater end plate, the rotor and brine end plate. The rotor contains some ducts in a circle which is the only rotating part of this device [21]. The end plate contains one in-port and one out-port. The RERD contains HP, LP and sealed zone [22,23]. When the rotor ducts are in HP zone, the HP brine through in-port of the brine end plate flow into the rotor ducts. The pressure energy of HP brine is transferred to LP seawater in a direct momentary contact, and the pressurized seawater discharge from out-port of the seawater end plate. When the rotor ducts are in LP zone, the LP seawater through in-port of the seawater end plate flow into the rotor ducts. The LP brine is pushed out through out-port of the brine end plate. As the rotor revolves, the ducts pass sealed zone that separates HP and LP zone.

The volumetric mixing expresses the volume of brine flowed out the RERD with the seawater from out-port of seawater end plate, which can be computed by the following equation [24]:

$$M = \frac{\left(S_{\text{HPS}} - S_{\text{LPS}}\right)}{\left(S_{\text{HPB}} - S_{\text{LPS}}\right)} \tag{1}$$

where M is volumetric mixing, S_{HPS} is HP seawater salinity, S_{LPS} is LP seawater salinity, and S_{HPB} is HP brine salinity. This equation applies when flow rate of HP stream is same as LP through RERD.

The mixing has no relation with the RERD efficiency, however, it is a loss in the overall SWRO system [25,26]. Because mixing will lead to the increase of the HP seawater salinity, so does the osmotic pressure and the production water cost [27–29]. Therefore, the mixing is a key parameter for RERD performance.

3. Numerical methods

3.1. Computational model

Fig. 2 shows the 3D simulation model of two-port RERD generated in the preprocessor ANSYS Workbench Design
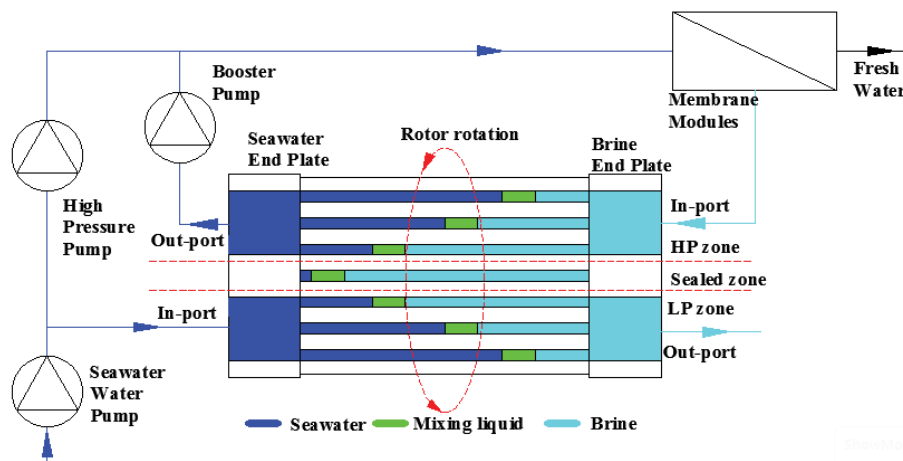

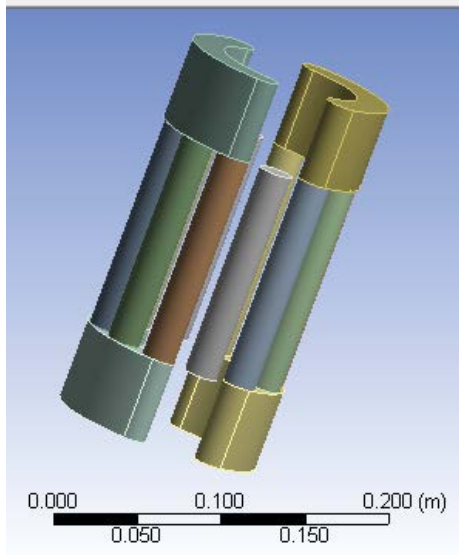Fig. 1. Operational principle of the SWRO with RERD.
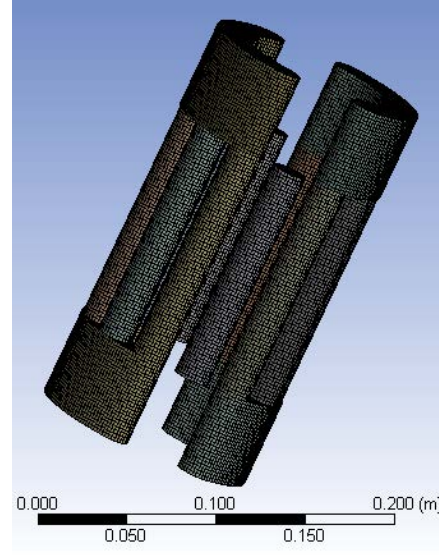
Fig. 2. Geometric model.

Fig. 3. Mesh model.

Modeler 14.5. The model was built on the basis of the four-port RERD [20]. This model has two sealed zones, different from the previous model which shows four zones. The structure of two-port RERD is same as the four-port, such as rotor duct number and diameter, rotor height and the acreage of one sealed zone. The clearance between the end plate and the rotor was unconsidered because of the extremely low leakage and simplify the computational model.

The mesh model was generated in the preprocessor ANSYS Workbench Meshing 14.5. Meshes were made by sweep method for rotor ducts and end plates. Fig. 3 shows the mesh model including hexahedral and wedge cells. The orthogonal quality was used to analyze the quality of the meshes. The minimum orthogonal quality was 0.67, which illustrated that the mesh was good [30].

3.2. Mathematical model

The continuity equation based on the mass conservation can be described as

$$\nabla \times \left(\rho \vec{v}\right) = 0 \tag{2}$$

where ρ is the density, kg/m^3; $\vec{v}$ is the velocity vector, m/s.

The momentum equation on the basis of the energy conservation is expressed as

$$\nabla \times \left(\rho \vec{v} \vec{v}\right) = -\nabla p + \nabla \times \left[\mu \left(\nabla \vec{v} + \nabla \vec{v}^T\right)\right] + \rho \vec{g} \tag{3}$$

where ∇p is the static pressure force, N; μ is the molecular viscosity, Pa·s; $\rho \vec{g}$ is the gravitational body force, N.

The turbulent viscosity, μ_t, in Eq. (4) can be obtained by the standard k-ε model which contains turbulent energy dissipation equation and turbulent kinetic energy equation.

$$\mu_t = \frac{c_\mu \rho k^2}{\varepsilon} \tag{4}$$

The turbulent kinetic energy equation provides

$$\frac{\partial(\rho k)}{\partial t} + \frac{\partial(\rho k u_i)}{\partial x_i} = \frac{\partial}{\partial x_j}\left[\left(\mu + \frac{\mu_t}{\sigma_k}\right)\frac{\partial k}{\partial x_j}\right] + G_k - \rho \varepsilon \tag{5}$$

The turbulent dissipation ratio equation is given as

$$\frac{\partial(\rho \varepsilon)}{\partial t} + \frac{\partial(\rho \varepsilon u_i)}{\partial x_i} = \frac{\partial}{\partial x_j}\left[\left(\mu + \frac{\mu_t}{\sigma_\varepsilon}\right)\frac{\partial \varepsilon}{\partial x_j}\right] + \frac{c_1 \varepsilon}{k} - c_2 \rho \frac{\varepsilon^2}{k} \tag{6}$$

where u_i is the time mean velocity, m/s; G_k represents turbulence kinetic energy, m^2/s^2; c_1 = 1.44, c_2 = 1.92, c_μ = 0.09, σ_k = 1.0, σ_ε = 1.3.

Mass transfer between seawater and brine can be solved in the transport equations of non-reacting species given as

$$\frac{\partial\left(\rho Y_i\right)}{\partial t} + \nabla \times (\rho \vec{v} Y_i) = -\nabla \times \left[-\left(\rho D_i + \frac{\mu_t}{\mathrm{Sc}_t}\right)\nabla Y_i\right] \tag{7}$$

where Y_i is mass fraction of species i; D_i is mass diffusion coefficient for species in mixture; Sc_t is turbulent Schmidt number and equal to 0.7 [31].

3.3. Mesh independent and experiment verification

Fig. 4 presents the effect of mesh number on the mixing at flow rate of 7.0 m^3/h and rotor speed of 300 rpm. As the mesh number increases, the mixing decrease first, and then keep at a stable level. When the mesh number increases from 1,057,778 to 1,890,069, the mixing changed from 7.01% to 6.93% and had little change. Thus, the mesh number used in the simulation was about 1,057,778.
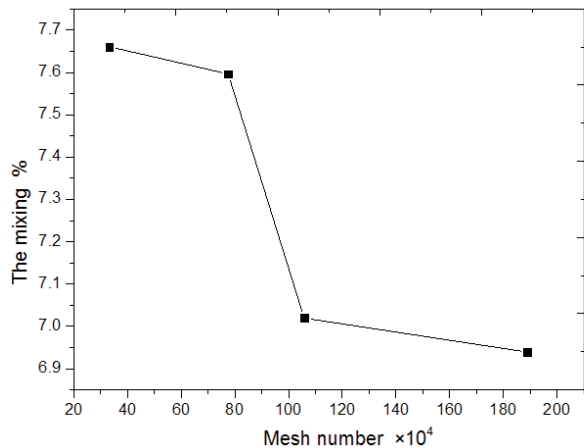
Fig. 4. Relation between the mixing and mesh number.

3.4. Simulation scheme

Eqs. (2)–(7) were computed in the FLUENT 14.5 based on the pressure-based solver. The gravitational acceleration was in view under the simulation. The PISO pressure-velocity coupling algorithm, standard pressure, first-order upwind discretization scheme turbulent for k and ε equations was utilized in calculation process. The moment equation and species transport equation chose second-order upwind discretization scheme. The interface is the contact surfaces between the rotor and two end plates to transfer the data. The rotor motion was simulated by the sliding mesh. For all the SM simulations, a time step needs to sweep an azimuthal angle of a cell. A time step half as large was also tested, however the results were identical.

The velocity-inlet and pressure-outlet was chosen as boundary conditions of in-ports and out-ports, respectively. The NaCl mass fractions of LP seawater and HP brine are 3.5% and 6.0%, respectively. Simulation model was filled with the LP seawater as the initial condition. The HP outlet salinity reaches a stable level and the flow rate is balanced for entering and leaving the model as the converged condition.

4. Results and discussion

4.1. Inflow length

Fig. 5 gives 2D salinity contour at rotor speed of 300 rpm and flow rate of 7.0 m³/h. The cutting plane was unfolded from a 3D central cylindrical surface with a diameter of 104 mm. From this figure, it can be seen that there is a mixing section separated seawater and brine in every rotor ducts. Due to the rotor rotation and the uneven velocity, the mixing section is irregular and has different shape in every rotor duct. The moving distant of mixing section is defined as inflow length (IFL) when rotor duct moves from the sealed area to next one. IFL directly affect the mixing and can be obtained according to the NaCl mass fractions of two rotor ducts in the sealed zone.

Fig. 6 presents the relation between the NaCl mass fraction and the height for two rotor ducts in sealed zone.
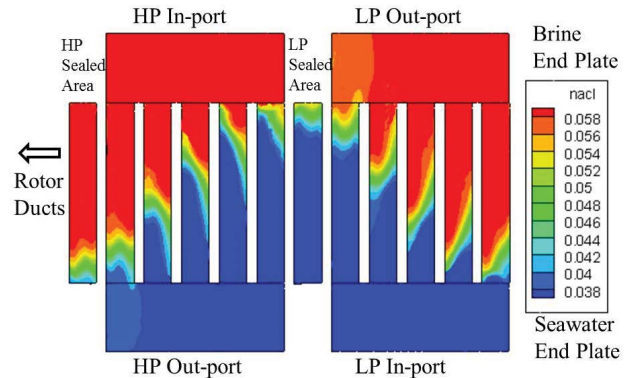

Fig. 5. 2D salinity contour of the central cylindrical surface.

The square points represent the rotor duct in HP sealed zone and the circle points show the rotor duct in LP sealed zone. The horizontal line represents the brine for the HP rotor duct and the seawater for the LP rotor duct, respectively. The incline line specifies the mixing section for HP and LP rotor duct. Two incline lines are almost parallel and the distant of two incline lines is IFL, just as shown in Fig. 6.

Fig. 7 descripts the relationship between reciprocal of rotor speed and IFL at flow rate of 7.0 m³/h for two-port and four-port RERD. From Fig. 7 and its fitting equation, IFL is positively proportional to reciprocal of rotor speed and increases with decrease of rotor speed for two-port and four-port RERD.

Fig. 8 shows the relationship between flow rates and IFL at rotor speed of 150 rpm for two-port and four-port RERD. From Fig. 8 and its fitting equation, it is clear that IFL is positively proportional to the flow rate and increases with the increasing of flow rate for two-port and four-port RERD.

From Figs. 7 and 8, the same conclusion that IFL of two-port RERD is longer than four-port RERD can be obtained at the same flow rate and rotor speed. The reason is that one port cover two rotor ducts for four-port RERD and five rotor ducts for two-port RERD. The time of two-port RERD
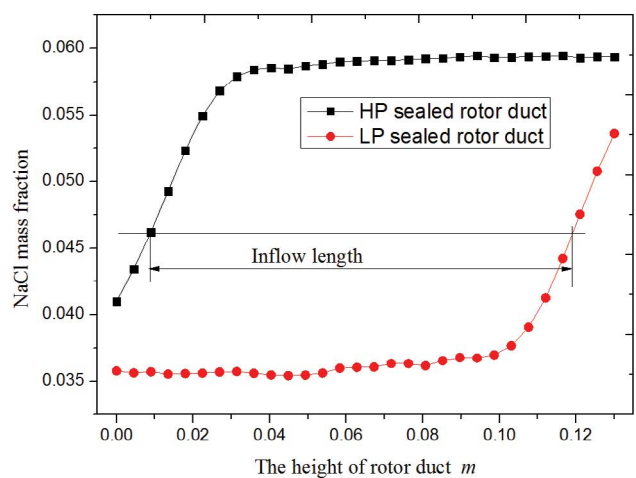

Fig. 6. Relation between the NaCl mass fraction and the height of rotor duct.
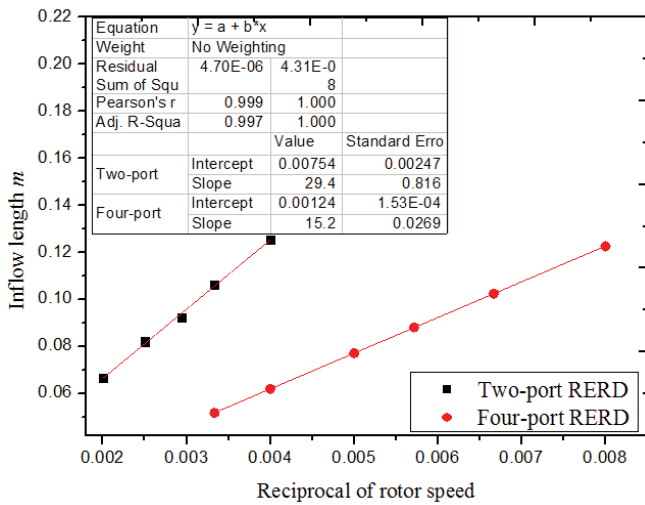
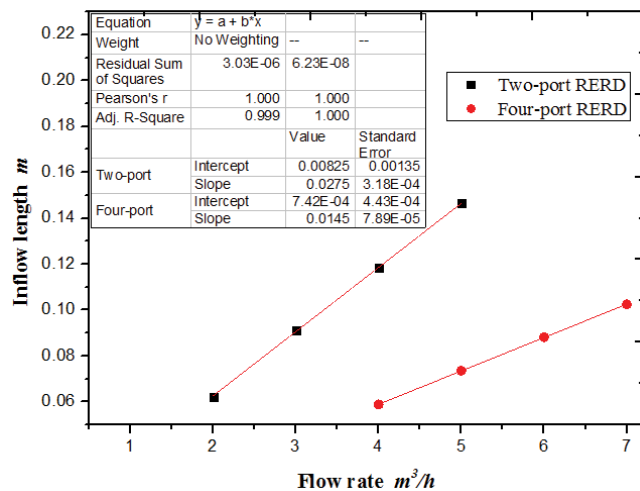Fig. 7. IFL at different reciprocal of rotor speed.

Fig. 8. IFL at different flow rate.

is about 2.5 times for four-port RERD when one rotor duct turns out one port at the same rotor speed. Another reason is that there are two HP/LP ports for four-port RERD, so the average velocity of four-port RERD is about 1.25 times for two-port RERD at the same flow rate. Combine the time and average velocity, IFL of two-port RERD is about twice as long as that of four-port RERD which is in accord with the slope of fitting equation. In addition, according to Figs. 7 and 8, the intercept of two-port RERD is almost equal to 0, so IFL also meets the theoretical Eq. (8)

$$l = \frac{\varphi Q(\alpha + \beta)}{120\pi m S n} \tag{8}$$

where n is the rotor speed, rpm; α is one port central angle; β is one rotor duct central angle; Q is brine flow rate, m³/h; S is one rotor duct area, m²; m is the minimum rotor duct number covered by one port, $m = 5$ for this device; φ is correction factor, in this paper $\varphi = 1.05$.
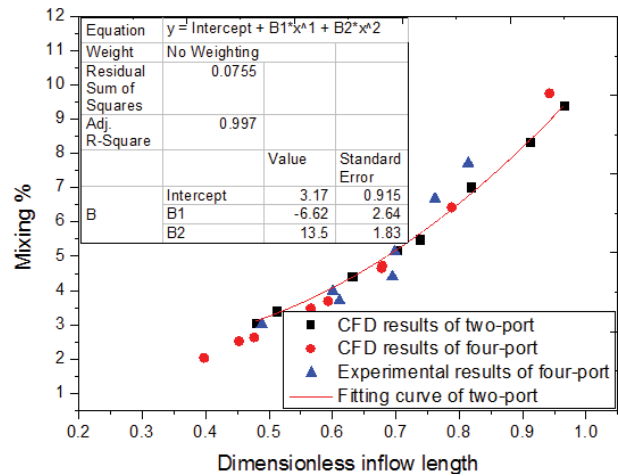

Fig. 9. Mixing at different dimensionless IFL.

4.2. Relationship between inflow length and mixing

The relationship between mixing and dimensionless IFL is shown in Fig. 9. Dimensionless IFL is defined as the ratio of IFL and rotor height. In this figure, the square points represent CFD results of two-port RERD whose fitting curve was also given, the circular points are CFD results of four-port RERD and the triangle points denote the experimental results of four-port RERD. The results of four-port RERD were shown in our previous research [20].

From Fig. 9 it can be seen that the mixing enhances with the increase of dimensionless IFL and has a polynomial relation with dimensionless IFL. The reason may be the irregular shape of mixing section caused by the rotation of the rotor in the rotor ducts shown in Fig. 5. The CFD results of four-port had been verified by the experimental results in our previous research, indicating that the simulation model and method results are feasible. This paper simulated the two-port RERD by the four-port RERD simulation method, so the simulation results of two-port RERD are reasonable.

In addition, two-port RERD has the same relation with four-port RERD. Based on the fitting equation of Fig. 9, when the mixing of two-port or four-port RERD is controlled in the level of 6%, dimensionless IFL must be less than 0.76. Combined with the difference of IFL between two-port and four-port RERD, four-port RERD is advantageous to keep the mixing in a less level under the same operation compared with two-port RERD. Thus four-port RERD would be the potential trend for the RERD.

5. Conclusion

For the sake of comparing the mixing behavior between two-port and four-port RERD, and four-port RERD, the simulation model of two-port RERD was built based on four-port RERD which had been validated in our previous research. The effects of operational conditions on the mixing of two-port RERD were simulated by the method of computational fluid dynamics.

New method was provided to calculate IFL according to the NaCl mass fractions of two rotor ducts in sealed zone.

IFL is inversely proportional to rotor speed and proportional to flow rate based on the simulation result. IFL of two-port RERD is twice as long as that of four-port RERD at the same rotor speed and flow rate.

Simulation results revealed that two-port RERD has the same polynomial relation with four-port RERD between mixing and dimensionless IFL. Four-port RERD can be beneficial to control the mixing in a low level under the same operational condition compared with two-port RERD. So four-port RERD is the potential trend for the RERD. The research gives some insights into the difference between two-port RERD and four-port RERD, and guides the design RERD in a low level mixing.

Acknowledgments

References

[1]   A. Zhu, P.D. Christofides, Y. Cohen, Effect of thermodynamic restriction on energy cost optimization of RO membrane water desalination, Ind. Eng. Chem. Res., 48 (2008) 6010–6021.
[2]   A. Zhu, P.D. Christofides, Y. Cohen, Energy consumption optimization of reverse osmosis membrane water desalination subject to feed salinity fluctuation, Ind. Eng. Chem. Res., 48 (2009) 9581–9589.
[3]   B. Qi, Y. Wang, S. Xu, Z. Wang, S. Wang, Operating energy consumption analysis of RO desalting system: effect of membrane process and energy recovery device (ERD) performance variables, Ind. Eng. Chem. Res., 51 (2012) 14135–14144.
[4]   L. Gao, A. Rahardianto, H. Gu, P.D. Christofides, Y. Cohen, Energy-optimal control of RO desalination, Ind. Eng. Chem. Res., 53 (2014) 7409–7420.
[5]   A. Zhu, P.D. Christofides, Y. Cohen, Minimization of energy consumption for a two-pass membrane desalination: Effect of energy recovery, membrane rejection and retentate recycling, J. Membr. Sci., 339 (2009) 126–137.
[6]   A. Zhu, P.D. Christofides, Y. Cohen, On RO membrane and energy costs and associated incentives for future enhancements of membrane permeability, J. Membr. Sci., 344 (2009) 1–5.
[7]   S. Bross, W. Kochanowski, N. El Maraghy, SWRO-core-hydraulic-system: first field test experience, Desalination, 184 (2005) 223–232.
[8]   D. Song, Y. Wang, S. Xu, Z. Wang, H. Liu, S. Wang, Control logic and strategy for emergency condition of piston type energy recovery device, Desalination, 348 (2014) 1–7.
[9]   E. Xu, Y. Wang, J. Zhou, S. Xu, S. Wang, Theoretical investigations on rotor speed of the self-driven rotary energy recovery device through CFD simulation, Desalination, 398 (2016) 189–197.
[10] E. Xu, Y. Wang, J. Wu, S. Xu, Y. Wang, S. Wang, Investigations on the applicability of hydrostatic bearing technology in a rotary energy recovery device through CFD simulation and validating experiment, Desalination, 383 (2016) 60–67.
[11] S. Bross, W. Kochanowski, Channel form for a rotating pressure exchange, U.S. Patent, 7815421, (2010).
[12] R.L. Stover, A. Ameglio, P.A.K. Khan, The Ghalilah SWRO plant: An overview of the solutions adopted to minimize energy consumption, Desalination, 184 (2005) 217–221.
[13] R.L. Stover, SWRO process simulator, Desalination, 221 (2008) 126–135.
[14] Y. Zhou, X. Ding, M. Ju, Y. Chang, Numerical simulation on a dynamic mixing process in ducts of a rotary pressure exchanger for SWRO, Desal. Wat. Treat., 1 (2009) 107–113.
[15] Y. Liu, Y.H. Zhou, M.S. Bi, 3D numerical simulation on mixing process in ducts of rotary pressure exchanger, Desal. Wat. Treat., 42 (2012) 269–273.
[16] R.L. Stover, Development of a fourth generation energy recovery device A 'CTO's Notebook', Desalination, 165 (2004) 313–321.
[17] S. Mambretti, E. Orsi, S. Gagliardi, R. Stover, Behaviour of energy recovery devices in unsteady flow conditions and application in the modelling of the Hamma desalination plant, Desalination, 238 (2009) 233–245.
[18] Z. Cao, J. Deng, W. Yuan, Z. Chen, Integration of CFD and RTD analysis in flow pattern and mixing behavior of rotary pressure exchanger with extended angle, Desal. Wat. Treat., 57 (2016) 15265–15275.
[19] Y. Wang, L. Wu, B. Li, W. Zhang, Y. Hu, Numerical simulation and analysis of the mixing process of rotary pressure exchangers with different sizes and structures, J. Chem. Eng. Jpn., 49 (2016) 573–578.
[20] E. Xu, Y. Wang, L. Wu, S. Xu, Y. Wang, S. Wang, Computational fluid dynamics simulation of brine–Seawater mixing in a rotary energy recovery device, Ind. Eng. Chem. Res., 53 (2014) 18304–18310.
[21] I.B. Cameron, R.B. Clemente, SWRO with ERI's PX pressure exchanger device — A global survey, Desalination, 221 (2008) 136–142.
[22] L. Wu, Y. Wang, E. Xu, J. Wu, S. Xu, Employing groove-textured surface to improve operational performance of rotary energy recovery device in membrane desalination system, Desalination, 369 (2015) 91–96.
[23] Y. Wang, Y. Duan, J. Zhou, S. Xu, S. Wang, Introducing pre-pressurization/depressurization grooves to diminish flow fluctuations of a rotary energy recovery device: Numerical simulation and validating experiment, Desalination, 413 (2017) 1–9.
[24] R.L. Stover, Seawater reverse osmosis with isobaric energy recovery devices, Desalination, 203 (2007) 168–175.
[25] B. Schneider, Selection, operation and control of a work exchanger energy recovery system based on the Singapore project, Desalination, 184 (2005) 197–210.
[26] S. Bross, W. Kochanowski, SWRO core hydraulic system: Extension of the SalTec DT to higher flows and lower energy consumption, Desalination, 203 (2007) 160–167.
[27] A.R. Bartman, A. Zhu, P.D. Christofides, Y. Cohen, Minimizing energy consumption in reverse osmosis membrane desalination using optimization-based control, J. Process. Contr., 20 (2010) 1261–1269.
[28] W. Qi, J. Liu, P.D. Christofides, Supervisory predictive control for long-term scheduling of an Integrated wind/solar energy generation and water desalination system, IEEE T. Contr. Syst. T., 20 (2012) 504–512.
[29] V.G. Gude, Energy consumption and recovery in reverse osmosis, Desal. Wat. Treat., 36 (2011) 239–260.
[30] ANSYS Meshing user's guide (release 14.5) ANSYS, Inc: Canonsburg, PA, USA, 2012.
[31] ANSYS Fluent user's guide (release 14.5) ANSYS, Inc: Canonsburg, PA, USA, 2012.